Magnetic exchange interactions and antiferromagnetism of ATcO$_3$ (A = Ca, Sr, Ba) studied from first principles

V. S. Borisov,[1,*] I. V. Maznichenko,[2] D. Böttcher,[1] S. Ostanin,[1] A. Ernst,[1] J. Henk,[2] and I. Mertig[1,2]

[1]*Max-Planck-Institut für Mikrostrukturphysik, Weinberg 2, D-06120 Halle, Germany*

[2]*Institut für Physik, Martin-Luther-Universität Halle-Wittenberg, D-06099 Halle, Germany*

The magnetic properties of ATcO$_3$ (A = Ca, Sr, Ba) perovskites were studied from first principles using multiple-scattering theory. For each system, the most preferable magnetic order is antiferromagnetic where the magnetic moments of the nearest Tc atoms are aligned antiparallel to each other. In the case of CaTcO$_3$ and SrTcO$_3$, their recently observed antiferromagnetism is supported by our calculation of the Tc-Tc exchange coupling parameters. The Néel temperatures T_N estimated for CaTcO$_3$ and SrTcO$_3$ are in a good agreement with experiment. For BaTcO$_3$, which is not synthesized so far, we predict a fundamental band gap of 0.3 eV and T_N below 900 K. In general, T_N increases with volume expansion, whereas the presence of vacancies on both the oxygen and cation sites of ATcO$_3$ should significantly suppress the critical temperature as well as the magnetic moment of Tc. Electronic correlations play a minor role in the formation of the magnetic state, although they may improve the calculated value of T_N.

I. INTRODUCTION

The magnetic properties of ABO$_3$ perovskites show an exceptional diversity, varying from a Pauli paramagnet to an antiferromagnetically ordered structure or a spin-spiral magnetic configuration.[1] The latter happens, for instance, in multiferroic TbMnO$_3$ below 28 K where the electronic order degrees in conjunction with cycloidal spin arrangement break inversion symmetry and create ferroelectric order due to the spin-orbit-related Dzyaloshinskii-Moriya exchange mechanism.[2] When the magnetic 3d atom occupies the B site of ABO$_3$, the perovskites frequently demonstrate robust ferromagnetism with a relatively high Curie temperature, for example, 280K for SrCoO$_3$. The experimental data widely presented in the literature indicate that, in contrast to 3d perovskites, the compounds with 4d and 5d cations on the B site display weaker tendency to magnetic order. This is due to their spatially extended d orbitals compared to the 3d orbitals. For instance, SrRuO$_3$ has a Curie temperature of 160K, which is far below room temperature, whereas SrMoO$_3$ is a Pauli paramagnet.

Recently, it has been reported that the Néel temperatures (T_N) of SrTcO$_3$ and CaTcO$_3$ reach surprisingly high values of 1000 and 800K, respectively.[3,4] Both compounds possess an orthorhombically distorted perovskite structure (*Pnma* symmetry), where the nearest Tc are ordered antiferromagnetically (AFM) to each other, forming the G-type AFM configuration similar to that in SrMnO$_3$ and CaMnO$_3$.[1] In SrTcO$_3$, the magnetic moment of Tc measured[3] at room temperature is 1.87 μ_B, which increases to 2.13 μ_B at 4K. Rodriguez and co-workers[3] have also suggested that the anomalously high T_N of SrTcO$_3$ is due to the particularly strong covalency of Tc–O bonds. The corresponding first-principles electronic-structure calculations[3] clearly demonstrate an extensive hybridization between the Tc 4d states and oxygen 2p states near the top of the valence band. A specific role of the 4d^3 electron configuration of SrTcO$_3$, which is in considerable contrast to those of SrMoO$_3$ and SrRuO$_3$, was also discussed by the authors of Ref. 3. Another group of authors[5] recently studied the series ATcO$_3$ (A = Ca, Sr, Ba) from first principles using a combination of the so-called Heyd-Scuseria-Ernzerhof (HSE) hybrid[6] density functional theory and Monte Carlo simulations, which yield the magnetic exchange coupling parameters and critical temperature. In ATcO$_3$, the resulting AFM ground state is characterized by large superexchange coupling (between -26 and -35 meV) and large T_N (between 750 and 1200K), which increase as a function of the A ionic radius.[5]

Further clarification of the mechanism which is responsible for the AFM order observed in SrTcO$_3$ and CaTcO$_3$ and their very high critical temperature requires a comprehensive first-principles analysis of the magnetic exchange interactions. Franchini *et al.*[5] argued that "the correct description of this complex class of materials can be only achieved within a beyond-local functional method such as HSE." In this study, we analyzed whether the three ATcO$_3$ (A = Ca, Sr, Ba) perovskites can be treated within the conventional local density approximation (LDA) and the generalized gradient approximation (GGA). We explored separately the magnetovolume effect and the effect of strong electronic correlations. Besides, for each system, we estimate its critical temperature T_N as a function of the concentration of intrinsic defects such as the cation and oxygen vacancies. The critical temperature was estimated within the mean-field approximation (MFA), the random phase approximation (RPA), and the Monte Carlo method.

The paper is organized as follows: In Sec. II, we introduce the details of the electronic-structure calculations concerning the crystal and magnetic structure of ATcO$_3$. Section III presents the obtained results and their analysis. First, we discuss the electronic structure and hybridization effects in ATcO$_3$, which are illustrated using the total and projected densities of states. Afterward, the main features and stability of the AFM ordering are considered using the evaluated exchange coupling parameters. Moreover, we simulated the effect of strong electronic correlations in the system using the Hubbard U parameter and calculated the Néel temperature

using different approaches. Next, we analyze the dependence of the magnetic properties of ATcO$_3$ on the unit-cell volume. Finally, we discuss the effect of oxygen and cation vacancies on the critical temperature and the magnetic moment of Tc. In Sec. IV, we summarize the results of our theoretical study.

II. DETAILS OF CALCULATION

To study an ATcO$_3$ family of perovskites, we employed density functional theory calculations within both the local density approximation and the generalized gradient approximation to the exchange-correlation potential.[7] The structural relaxation was performed using the Vienna *ab initio* simulation package (VASP).[8–10] The electron-ion interactions were described by projector-augmented-wave pseudopotentials, and the electronic wave functions were represented by plane waves with a cutoff energy of 450 eV. For the ionic relaxation, the Γ-centered and dense Monkhorst-Pack[11] **k** mesh was used. The ionic relaxation was performed until the forces were less than 5×10^{-3} eV/ Å.

The magnetic cell of ATcO$_3$ can be defined by the parameters $a \approx b \approx \sqrt{2}a_p$ and $c \approx 2a_p$, where a_p is the cubic lattice parameter of one formula unit ABO_3, as shown in Fig. 1. This cell contains four formula units of ATcO$_3$. For A = Ca, Sr, Ba, the use of the GGA yields the equilibrium volumes of 242.44 Å^3, 251.39 Å^3, and 266.08 Å^3 per magnetic unit cell, respectively. Using the LDA, we obtained for each A = Ca, Sr, Ba the equilibrium volume of 228.42 Å^3, 236.45 Å^3 and 250.43 Å^3, respectively. In the case of SrTcO$_3$ (CaTcO$_3$), the experimental volume is 244.3 Å^3 (231.2 Å^3) per cell. Thus, the GGA option overestimates the volume by 3%–5%, while LDA underestimates it by approximately the same values. The use of the HSE hybrid scheme, which goes beyond the LDA/GGA standard, allows us to improve the agreement between the experimental and theoretical volumes of ATcO$_3$. For instance, Franchini *et al.*,[5] using a mixing parameter $\alpha = 0.1$, obtained for SrTcO$_3$ (CaTcO$_3$) the volume of 244.2 Å^3 (229.0 Å^3), while their predicted volume of BaTcO$_3$ is 259.6 Å^3. In this paper, we focus mainly on the GGA results since the LDA

fails to reproduce the fundamental band gap of CaTcO$_3$ and reduces the band gap of SrTcO$_3$ by ∼0.5 eV as compared to the GGA. For SrTcO$_3$ after relaxation, the cell-parameter ratios b/a and c/a, as well as the atomic positions, are in reasonably good agreement with the available experimental data.[3]

For a given volume of the unit cell, we also investigated the effect of correlations on the orbitals hybridization and the parameters of the antiferromagnetic state using the GGA + U approximation (Hubbard model).[12] More specifically, we introduced an additional splitting between occupied and unoccupied technetium $4d$ states, which, according to earlier works by Rodriguez *et al.*, show a high degree of hybridization with oxygen $2p$ orbitals.

The magnetic properties of ATcO$_3$ were computed using multiple-scattering theory based scalar-relativistic Green's function technique,[13] which is known also as the Korringa-Kohn-Rostoker (KKR) method.[14,15] The atomic sphere approximation to the crystal potential was applied, as well as the full charge density KKR option. For the Brillouin zone integration during self-consistent calculations, a special 12 × 12 × 10 **k**-point mesh was utilized. The results were carefully checked with respect to the **k** mesh and the maximal angular momentum used. The magnon spectra calculations, which involve the critical temperature estimates, were performed using a dense 24 × 24 × 20 **k**-point mesh.

For the three types of magnetic order of each perovskite, we examined their total energies. To properly treat the energy of the paramagnetic solution, we used the disordered local moment (DLM) theory within the coherent-potential approximation (CPA), as implemented in multiple-scattering theory (KKR-CPA).[16–18] Aside from a comparative energetics, the preferable magnetic order of ATcO$_3$ can be evaluated using the effective parameters of the magnetic exchange interactions, which are known to quantify the magnetic ground state of the crystal. These parameters were obtained using the magnetic force theorem[19] and the effective classical Heisenberg Hamiltonian

$$H = -\sum_{i,j} J_{ij}\, \mathbf{e}_i \cdot \mathbf{e}_j, \qquad (1)$$

where i and j number the magnetic cations, and $\mathbf{e}_i$ is a unit vector in the direction of the magnetic moment of the i th atom. The critical temperature estimates were obtained, first, using the mean-field approximation and then also within the RPA and the Monte Carlo method. This technique was successfully applied to diluted magnetic semiconductors, digital magnetic alloys, and magnetically doped oxides.[20,21] The most reliable T_N values were obtained within the Monte Carlo method in combination with the DLM theory. This issue was discussed in the literature.[22,23]

The intrinsic point defects of ATcO$_3$, namely, the vacancies were modeled within the CPA that implies randomly distributed vacancies over all atomic sites of the given species. For each perovskite ATcO$_{3-y}$, the concentration of oxygen vacancies varies between $y = 0$ and $y = 0.45$ per formula unit. Regarding the cation vacancies in A_{1-x}Tc$_{1-x}$O$_3$, their concentrations were modeled in the range of $0 < x < 0.1$ per formula unit. Although such cation-deficient perovskites are
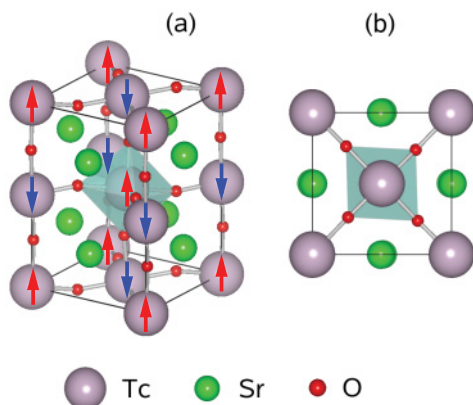

FIG. 1. (Color online) Side (a) and top (b) view of the G-type AFM cell of SrTcO$_3$. In panel (a), the magnetic moments of Tc directed upward (downward) along the [001] axis are indicated by red (blue) arrows.

usually referred to in the literature as $ABO_{3+\delta}$, it should be noted that the bulk perovskite structure is actually unable to accommodate interstitial oxygen.

According to the previous report on ATcO$_3$, we considered the three magnetic configurations, namely, the so-called A-, C-, and G-type AFM ordering, which are shown in Fig. 9 of Ref. 3. After a structure relaxation, the A-type configuration, with the ferromagnetically ordered sheets of Tc moments stacked antiferromagnetically along [010], becomes nonmagnetic, whereas the two others result in the AFM solution. This is in complete agreement with *ab initio* calculations reported by Rodriguez *et al*. The C-type structure, where the ferromagnetic sheets of Tc moments are aligned along [100], shows the low-spin Tc moment below $0.7\mu_B$. However, the G-type AFM ordering is energetically favorable by 0.29 eV/cell compared to that of C type. In the G-type configuration, all nearest Tc are ordered antiferromagnetically to each other, as shown in Fig. 1. This G-type ATcO$_3$ cell, which contains four Tc atoms with the moments oriented along [001], is used for further calculations of the magnetic exchange interactions and critical temperature.

III. RESULTS AND DISCUSSION

A. Electronic structure

In Fig. 2, we plot the total density of states (DOS) for the three compounds ATcO$_3$. The densities of states calculated for the G-type AFM configuration reveal the insulating behavior for the perovskites. Thus, ATcO$_3$ is a typical antiferromagnetic
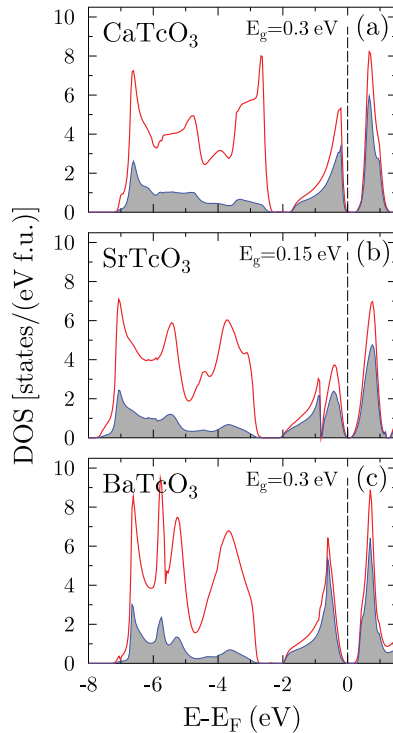

FIG. 2. (Color online) Total density of states of ATcO$_3$ (A = Ca, Sr, Ba) and the contribution of the magnetic technetium cations (shaded area) calculated in the G-type magnetic configuration after relaxation within the GGA. The band gaps E_g are given for each material.
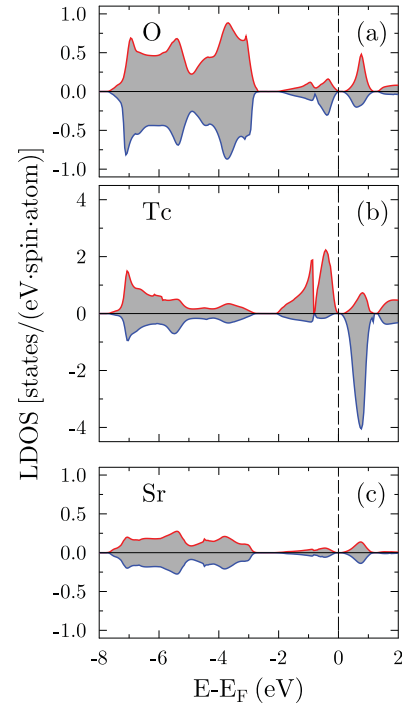

FIG. 3. (Color online) The site-projected density of states of SrTcO$_3$ in the G-type relaxed structure. For Tc, the spin-up and -down DOS are plotted in the middle panel by red and blue lines, respectively. Each magnetic cell contains four Tc, two of which have the spin DOS in reverse.

Slater insulator. Using the GGA, we obtained a band gap E_g between 0.15 and 0.3 eV in a row A = Ca, Sr, Ba, which are similar to the results calculated by Rodriguez *et al*.[3] The LDA systematically underestimates E_g. In the case of CaTcO$_3$, this option seems to be inappropriate since LDA results in a metallic gapless band structure. It should be noted that E_g, calculated by Franchini *et al*.[5] within the parametric HSE scheme, is five times larger then our GGA result, while the corresponding experimental data for the gap values are not known so far. It would be also worthwhile to know whether this rather small $E_g \leqslant 0.3$ eV predicted for ATcO$_3$ is essentially independent of temperature below T_N. Meanwhile, the width of the valence band of ATcO$_3$, as shown in Fig. 2, is typically wide, varying slightly at around 8 eV. This wide occupied band of technetium perovskites may indicate that any further theoretical work beyond the local spin density approximation, such as a self-interaction correction and the Hubbard U parametrization, is not obligatory, especially because there are no experimental data by which these corrections can be confirmed.

In Fig. 3, we plot the site-projected DOS of SrTcO$_3$, which is typical for these perovskites. In all ATcO$_3$ perovskites, the top occupied DOS near the Fermi energy E_F is formed by strongly hybridized Tc $4d$ and oxygen $2p$ states, as shown in Fig. 3, whereas the cation A contributes insignificantly between $E = -3$ eV and 0. Since the Tc cation, with its electronic configuration $4d^3$, is nominally in the oxidation state 4+, one can expect that the Tc–O bonds are not purely ionic. Instead, these bonds show a degree of covalency. This issue was well discussed in Ref. 3.

The electronic structure of the ATcO$_3$ perovskites is very similar to that of ruthenium-based perovskites, ARuO$_3$, with the only difference that Ru has one $4d$ level more occupied.[24,25] This additional electron in ARuO$_3$ leads to a stronger covalency between Ru $4d$ and O $2p$ states, making these compounds *bad metals*. As a result, oxygen states have more weight close to the Fermi level, contributing significantly to the Stoner parameter and favoring ferromagnetic or paramagnetic order.[25] In ATcO$_3$, the oxygen states are as well weakly spin polarized, but the effect is much smaller than in the ruthenium-based perovskites. Consequently, the superexchange mechanism is dominantly responsible for the antiferromagnetic order in ATcO$_3$.

B. Magnetic exchange interactions

To illustrate the AFM order, which is observed for the G-type ATcO$_3$, we calculated the magnetic exchange coupling parameters. These parameters are plotted in Fig. 4 versus the Tc-Tc distance d. All three curves seen in Fig. 4 indicate the existence of a pronounced AFM coupling between the nearest Tc atoms separated by the distance of about 7.5 Å. The corresponding magnitudes J_{01} are negative and spread around -15 meV. Contrary to J_{01}, the magnetic coupling with the second Tc neighbor J_{02} is ferromagnetic, with the positive magnitude ranging slightly between 1.9 and 2.3 meV for the different A species. Thus, J_{02} also favors the G-type AFM order since the second coordination shell represents the sublattice with the same orientation of magnetic moment as that of Tc at the origin. For comparison, the corresponding J_{02} values shown in Ref. 5 are negative for CaTcO$_3$ and SrTcO$_3$ whereas for BaTcO$_3$, $J_{02} > 0$. The more distant Tc ($i > 2$) contribute marginally to the cumulative exchange parameter $J_0 = \sum_i J_{0i}$. As a result, J_0 attains a significantly negative value, thereby confirming the stability of the G-type antiferromagnetism for ATcO$_3$. These findings support the total energy calculations which show that the G-type structure has the lowest energy compared to the A- and C-type magnetic configurations. It should be noted that the direct magnetic coupling between Tc is mediated in ATcO$_3$ by oxygen anions and, therefore, the magnetic exchange mechanism of ATcO$_3$ is a classical example of superexchange, which results in antiferromagnetism. The Goodenough-Kanamori rules[26]
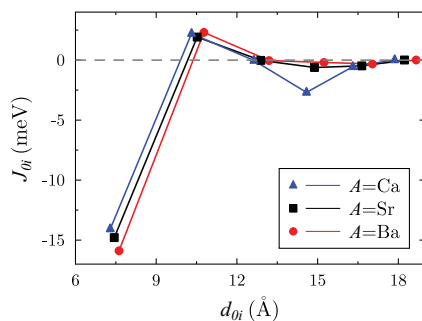

FIG. 4. (Color online) The magnetic exchange coupling parameters J_{0i} (in meV) calculated for ATcO$_3$ (A = Ca, Sr, Ba) and plotted as a function of the Tc-Tc separation. The data are calculated for the relaxed G-type antiferromagnetic ATcO$_3$ with the lattice parameters $a = b = c/\sqrt{2}$.
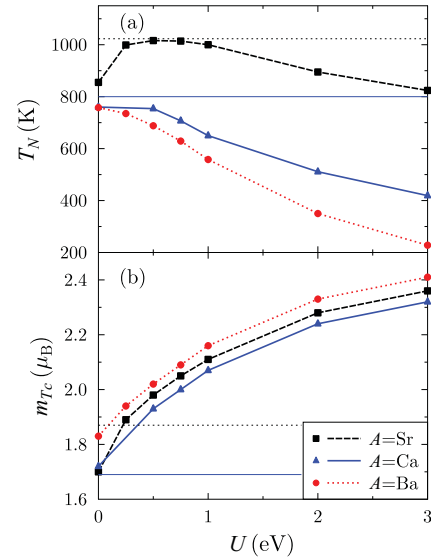

FIG. 5. (Color online) The mean-field estimates of T_N (a) and technetium magnetic moments m_{Tc} (b), calculated for each ATcO$_3$ (A = Ca, Sr, Ba) in the G-type AFM configuration, are plotted as a function of the model parameter U. Experimental values of the magnetic parameters for SrTcO$_3$ and CaTcO$_3$ are indicated by black dashed and blue solid horizontal lines, respectively.

applied to the less than half-filled $4d$ orbitals of Tc support this picture.

C. Effect of electronic correlations

In this section, we consider the impact of electronic correlations on electronic and magnetic properties of ATcO$_3$ perovskites studied within the LDA $+ U$ method.[27] The LDA $+ U$ method allows us to mimic in a simple manner electronic correlations by shifting and localizing particular electronic states using a constant potential specified by the parameter U. In the ATcO$_3$ systems, this potential is applied to the occupied Tc $4d$ states. The critical temperature in the mean-field approximation and magnetic moments residing on the technetium cations are plotted in Fig. 5 as a function of U. In the case of ATcO$_3$ perovskites, the T_N^{MFA} represents the effective exchange parameter. For all three perovskites, the magnetic moments of the technetium atoms increase monotonically as U increases. The same tendency was found for the size of the band gap. This can be explained by narrowing the bands and shifting occupied $4d$ states down in energy. The critical temperatures of CaTcO$_3$ and BaTcO$_3$ are reduced with increasing U, while that of SrTcO$_3$ has a more complicated behavior. It reaches a maximum at $U = 0.5$ eV and then drops, similar to other cases.

To illustrate the effect of correlations on the electronic structure, we plot the total and site-projected densities of state (Fig. 6) for SrTcO$_3$ with the experimental volume for two values of the parameter U: 0.0 and 0.5 eV. It appears that the introduction of splitting U leads to a shift of the states near the Fermi level so that the energy gap between occupied and unoccupied states becomes significantly larger ($E_g = 0.4$ eV). The corresponding experimental data are expected to determine the actual size of the fundamental gap and thereby
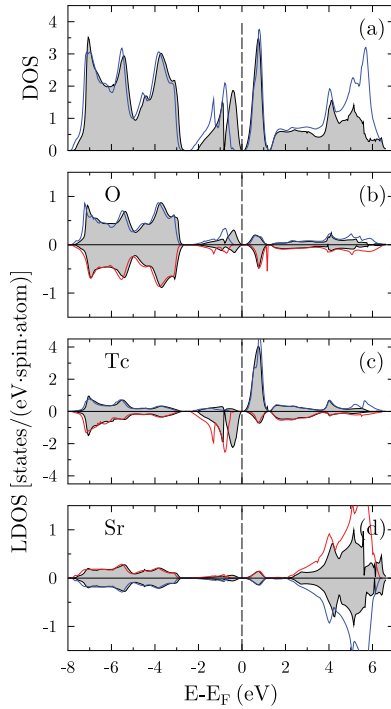
FIG. 6. (Color online) The total and site-projected densities of states of $SrTcO_3$ in the G-type state without correlations (shaded area) and with correlations corresponding to $U = 0.5$ eV (color lines). For each atom, the spin-up and -down DOS are plotted by red and blue lines, respectively.

clarify the contribution of the electronic correlations to the unusual magnetic phenomena in the considered transition-metal oxides.

Since all three compounds differ mainly by the behavior of $4d$ electrons close to the Fermi level (see Fig. 2), one can conclude that there is a certain degree of hybridization between Tc $4d$ and O $2p$ states at which the critical temperature has a maximum. A weaker or a stronger hybridization leads to decreasing exchange parameters. As it is shown later, in realistic simulations of T_N, this optimum is reached already by means of the GGA. So, we conclude that the magnetic properties of the transition-metal perovskites $ATcO_3$ can be successfully described without inclusion of additional correlation effects, although they can provide some valuable corrections to the critical temperature and increase the fundamental gap.

D. Calculation of T_N beyond the mean-field approximation

In addition to the results discussed above, we performed calculations of the Néel temperature using more sophisticated models: the first one is the RPA within $GGA + U$ and the second model is the Monte Carlo method. The corresponding RPA and Monte Carlo estimates of T_N are presented in Figs. 7 and 8, respectively. The Néel temperature is plotted as a function of the parameter U. From Fig. 7 it is seen that the use of RPA systematically decreases T_N by ~ 300 K compared to that of MFA, while the results of Monte Carlo simulations obtained for the AFM solution show no significant changes compared to that of RPA. At the same time, we observe a
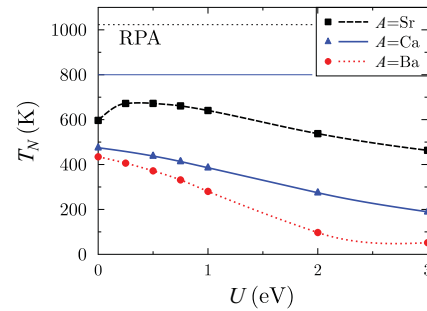

FIG. 7. (Color online) The Néel temperature estimates T_N calculated within RPA for each $ATcO_3$ ($A =$ Ca, Sr, Ba) as a function of the model parameter U. Experimental values of T_N for $SrTcO_3$ and $CaTcO_3$ are indicated by black dashed and blue solid horizontal lines, respectively.

pronounced reduction of T_N with the parameter U, which can be related to the specific features of the orbital hybridization in $4d$ perovskites as discussed above, whereas for $3d$ magnetic perovskites the magnetic ordering is known to become stronger with increasing U.

Up to now, all presented critical temperatures were calculated from exchange parameters obtained for an antiferromagnetic reference system at $T = 0$ K. For systems with a low critical temperature, this approach is appropriate. However, with increase of temperature, the exchange parameters can be significantly modified. This can be taken into account within the disordered local moment theory.[18,22,23,28] Meanwhile, the DLM solution for $SrTcO_3$ makes the value of T_N very close to the experimentally obtained value (see Fig. 8). The value of the parameter U of around 0.5 eV seems to provide the best agreement with available experimental data.

The feasibility of robust antiferromagnetism of $ATcO_3$ perovskites was to our knowledge never discussed. Currently, the attention to the high-T_N compensated antiferromagnets is very limited. However, these materials can be used as AFM substrates, with TcO_2 interfacial termination. Such composite materials are extremely important for applications in spintronics which utilize the anisotropic tunneling magnetoresistance.
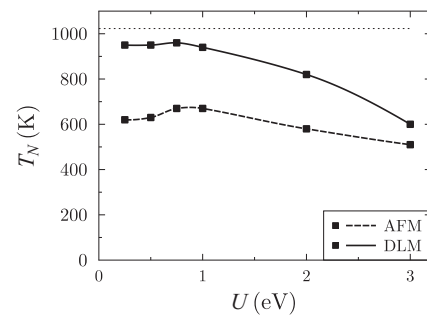

FIG. 8. The Néel temperature estimates T_N calculated using the Monte Carlo method for $SrTcO_3$ as a function of the model parameter U. The values obtained within DLM are compared to that of the completely ordered system (AFM). The experimental value of T_N for $SrTcO_3$ is indicated by the black dashed line.
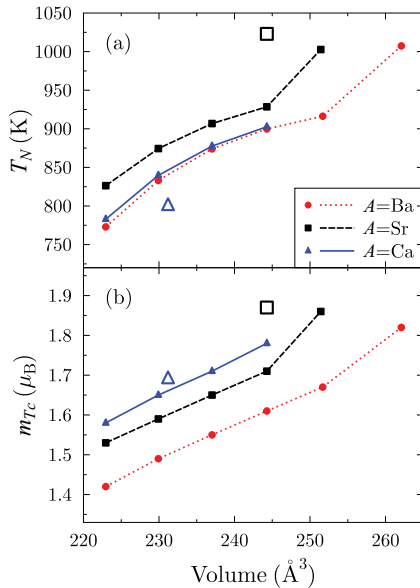
FIG. 9. (Color online) The mean-field estimates of T_N (a) and technetium magnetic moments m_{Tc} (b), calculated for each ATcO$_3$ (A = Ca, Sr, Ba) in the G-type AFM configuration, are plotted as a function of the unit-cell volume. The open square and triangle correspond to the experimental values of m_{Tc} and T_N: □, Ref. 3 for SrTcO$_3$; △, Ref. 4 for CaTcO$_3$.

E. Magnetovolume effect

To reveal the magnetovolume effect for each perovskite ATcO$_3$, we calculated within MFA the critical temperature T_N and the magnetic moment of Tc as a function of the G-type unit-cell volume. The results are plotted in the two panels of Fig. 9. For each ATcO$_3$, the calculated magnetic moments of Tc increase almost monotonously with the volume increase up to the equilibrium GGA volume, as shown in Fig. 9(b). In the case of CaTcO$_3$, the magnetic moment value $m_{Tc} \sim 1.7\mu_B$, which is calculated at the experimental volume, is in a good agreement with the measurements.[4] For SrTcO$_3$, the Tc moment calculated at the equilibrium GGA volume almost reaches the room-temperature experimental value of 1.87 μ_B. In BaTcO$_3$, we estimate the m_{Tc} value of $\sim 1.8\mu_B$. The use of the HSE hybrid scheme can enhance the calculated Tc moment. In particular, Franchini *et al.*[5] report $m_{Tc} \sim 2.0\mu_B$ for each system. The MFA critical-temperature estimates plotted in Fig. 9(a) behave similarly to that of m_{Tc}: there is a noticeable increase of T_N with the volume. Since Franchini *et al.*[5] obtained enhanced Tc moments, their T_N estimates are systematically larger compared to our results. Nevertheless, there is reasonably good agreement between the two different schemes of density functional theory.

The effect of the T_N enhancement in ATcO$_3$ can be understood if we consider the hybridization between the Tc d states and p orbitals of neighboring oxygen.[29] In ATcO$_3$, the large extent of $4d$ orbitals leads to a relatively high degree of covalency of the Tc–O bonds. The hybridization depends on the orbital spatial extent and also on the interatomic separation. The Tc magnetic moment increases constantly with the distance between the ions. The $4d$ states close to the Fermi level start to drift toward the O $2p$ states,
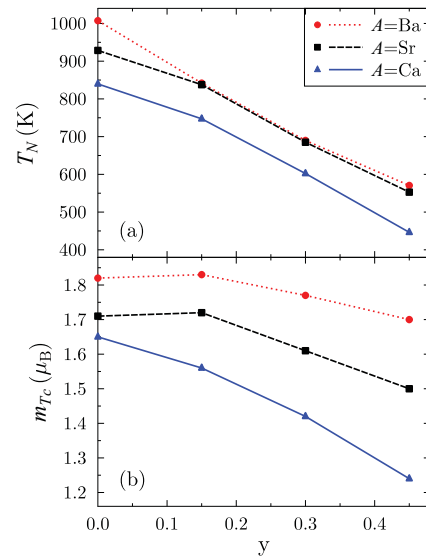

FIG. 10. (Color online) The Néel temperature estimates T_N and magnetic moments m_{Tc} of ATcO$_{3-y}$ (A = Ca, Sr, Ba) are plotted versus the O-vacancy concentration y in the panels (a) and (b), respectively.

narrowing the bandwidth and enhancing by this the effect of the hybridization, which is very similar to the LDA + U results. This rearrangement of levels leads to an increase of the effective exchange parameters. However, similar to the LDA + U case, we found that from a certain volume, the exchange parameters start to decrease, reducing thereby the critical temperature (not shown in Fig. 9).

In a recent paper (Ref. 5), the issue of the Tc–O bond lengths as well as the Tc–O–Tc bond angles were discussed. The Tc–O–Tc angles steeply stretch from $\sim 150°$ to $\sim 170°$ and then to $\sim 179°$ when A changes from Ca→Sr→Ba. The larger the Tc–O–Tc angles, the larger superexchange coupling and, therefore, the larger T_N. This increase of T_N correlates with a progressive reduction of the structural Jahn-Teller distortions.[5]

F. Effect of cation and oxygen vacancies

The electronic character of Tc–O bonds seems to be essential for the robust antiferromagnetism of ATcO$_3$. It is known, however, that an oxygen vacancy is a rather common defect in perovskites. From this point of view, it is important to examine the O-deficient ATcO$_{3-y}$ systems. Here, we investigate the effect of oxygen vacancies on the Tc magnetic moment and Néel temperature of ATcO$_{3-y}$. In general, anion-deficient perovskites are of significant interest as ionic conductors. Although some perovskites, such as SrTiO$_{3-y}$, demonstrate the room-temperature solid solution of randomly distributed O vacancies over the range $0 \leqslant y \leqslant 0.5$, we realize that even some moderate concentration of O vacancies in ATcO$_{3-y}$ may drastically change the magnetic order and oxidation state of Tc.

The results for the Tc magnetic moment and T_N of ATcO$_{3-y}$ are collected in Fig. 10. All T_N estimates were obtained within the MFA. The O vacancy concentration y varies between $y = 0$ and 0.45 per formula unit. More specifically, each O site in the supercell contains the same portion of
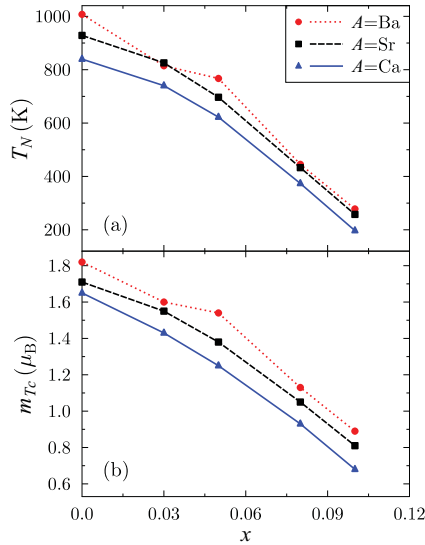
FIG. 11. (Color online) The mean-field estimates of T_N (a) and Tc magnetic moment (b) of $A_{1-x}Tc_{1-x}O_3$ (A = Ca, Sr, Ba) calculated as a function of the cation-vacancy concentration x.

vacancy $\square_O$, while the largest modeled concentration is 15 at.%. It is naturally expected that the presence of $\square_O$ weakens the magnetic moment of Tc. Indeed, the relative decrease of m_{Tc} seen in Fig. 10 can reach 20%–25% for the largest examined concentration of $\square_O$. However, the calculated critical temperature decreases almost twice as much as m_{Tc} with the increase of the $\square_O$ concentration. Nevertheless, we estimate that for all three $ATcO_{3-y}$ materials, their T_N may be higher than 500 K even for the upper $\square_O$ limit known for perovskites.

We simulated the effect of cation vacancies on the magnetic moment formation and critical temperature of $A_{1-x}Tc_{1-x}O_3$. In this case, each cation site A and B has the same deficiency. The cation vacancy concentration was varied between $0 < x < 0.1$. The results are plotted in Fig. 11. Contrary to the results plotted in Fig. 10, the presence of vacancies on the cation sites significantly suppresses the magnetic moment of Tc to values below 1 μ_B, seen at $x = 0.1$ in Fig. 11. The Néel temperature of $A_{1-x}Tc_{1-x}O_3$ falls below room temperature at the composition $x = 0.1$. This seems to be quite obvious since both the critical temperature and overall stability of the AFM order strongly depend on the ideal periodic arrangement of the magnetic technetium sublattice. As is shown in Fig. 4, the magnetic ordering of $ATcO_3$ stems from the strongly antiferromagnetic exchange interaction between the nearest Tc atoms. When the local moment of Tc is suppressed by a vacancy, the exchange coupling of Tc becomes weaker and, as a result, T_N decreases. The role of vacancies on the A sites is obviously marginal for the magnetic properties of $ATcO_3$ since the A sites have no induced magnetic moment.

IV. SUMMARY

We have studied the electronic structure and magnetic properties of technetium perovskites $ATcO_3$ (A = Ca, Sr, Ba) from first principles, using multiple-scattering theory together with the coherent-potential approximation to density functional theory. It was confirmed that the ground state for each $ATcO_3$ material is the G-type antiferromagnetic structure, where the nearest Tc magnetic moments are oriented antiparallel to each other. The spatial picture of the magnetic exchange interactions, calculated between Tc on the basis of the magnetic force theorem within the effective Heisenberg Hamiltonian, shows an oscillating behavior and thereby confirms the G-type antiferromagnetism in $ATcO_3$.

For CaTcO$_3$ and SrTcO$_3$, our T_N estimations of 840 and 930 K, respectively, are in agreement with the experiment. We also suggest that BaTcO$_3$ with $T_N \sim 1000$ K, which is not synthesized so far, could be a material of fundamental interest. For each perovskite, its critical temperature increases with increasing volume. The effect was analyzed in terms of the electronic degrees of freedom. There is a pronounced overlap of the technetium $4d$ orbitals and oxygen p orbitals, which form the top of the valence band. Electronically, the Tc–O bonds have an extra degree of covalency due to the $4d^3$ configurations of Tc, which is nominally in 4+ state. These factors mediate direct Tc-Tc coupling by the strong superexchange mechanism. We predict that the insulating band gap of $ATcO_3$ may vary between 0.15 and 0.3 eV.

We modeled the effect of both the oxygen and cation vacancies on the magnetic properties of $ATcO_3$. It was found that the presence of the oxygen vacancies below 10 at.% is less critical for the reduction of T_N and the magnetic moment of Tc than the similar amount of the cation vacancies which may reduce T_N below room temperature. In the latter case, the long-range magnetic ordering between Tc is broken by the cation vacancy on the Tc sublattice. Regarding the O vacancies in the system, we suggest that their presence below 10 at.% may keep the system strongly antiferromagnetic with $T_N \sim 500$ K.

The role of electronic correlations in the particular magnetic ordering observed in experiment for $ATcO_3$ was analyzed using a semiempirical GGA + U method, which allowed us to investigate the relation between the orbitals hybridization and the magnetic parameters of the considered oxides. It appeared that due to correlations, d orbitals of technetium cations and p ligand orbitals shift with respect to each other, thereby enhancing the local magnetic moments and, consequently, the critical temperature.

Our comparative study of the estimates of the Néel temperature, obtained within the mean-field theory, random phase approximation, and Monte Carlo simulations, showed that the last one combined with the DLM theory and the Hubbard model for the electronic correlations provides a satisfying agreement with experimental data. In view of possible applications of the strong high-temperature antiferromagnetism of the studied perovskites in spintronics, further experimental work on the subject would significantly improve the understanding of the observed magnetic phenomena.

*vborisov@mpi-halle.mpg.de

[1] J. B. Goodenough, Rep. Prog. Phys. **67**, 1915 (2004).

[2] S. Picozzi and C. Ederer, J. Phys.: Condens. Matter **21**, 303201 (2009).

[3] E. E. Rodriguez, F. Poineau, A. Llobet, B. J. Kennedy, M. Avdeev, G. J. Thorogood, M. L. Carter, R. Seshadri, D. J. Singh, and A. K. Cheetham, Phys. Rev. Lett. **106**, 067201 (2011).

[4] M. Avdeev, G. J. Thorogood, M. L. Carter, B. J. Kennedy, J. Ting, D. J. Singh, and K. S. Wallwork, J. Am. Chem. Soc. **133**, 1654 (2011).

[5] C. Franchini, T. Archer, J. He, X.-Q. Chen, A. Filippetti, and S. Sanvito, Phys. Rev. B **83**, 220402 (2011).

[6] J. Heyd, G. E. Scuseria, and M. Ernzerhof, J. Chem. Phys. **118**, 8207 (2003).

[7] J. P. Perdew and Y. Wang, Phys. Rev. B **45**, 13244 (1992).

[8] G. Kresse and J. Hafner, Phys. Rev. B **49**, 14251 (1994).

[9] G. Kresse and J. Furthmüller, Phys. Rev. B **54**, 11169 (1996).

[10] J. Hafner, J. Comput. Chem. **29**, 2044 (2008).

[11] H. J. Monkhorst and J. D. Pack, Phys. Rev. B **13**, 5188 (1976).

[12] V. I. Anisimov, J. Zaanen, and O. K. Andersen, Phys. Rev. B **44**, 943 (1991).

[13] M. Lüders, A. Ernst, W. M. Temmerman, Z. Szotek, and P. J. Durham, J. Phys.: Condens. Matter **13**, 8587 (2001).

[14] J. Korringa, Physica (Amsterdam) **13**, 392 (1947).

[15] W. Kohn and N. Rostoker, Phys. Rev. **94**, 1111 (1954).

[16] B. L. Gyorffy, Phys. Rev. B **5**, 2382 (1972).

[17] T. Oguchi, K. Terakura, and N. Hamada, J. Phys. F: Met. Phys. **13**, 145 (1983).

[18] B. L. Gyorffy, A. J. Pindor, J. Staunton, G. M. Stocks, and H. Winter, J. Phys. F: Met. Phys. **15**, 1337 (1985).

[19] A. I. Liechtenstein, M. I. Katsnelson, V. P. Antropov, and V. A. Gubanov, J. Magn. Magn. Mater. **67**, 65 (1987).

[20] D. Ködderitzsch, W. Hergert, W. M. Temmerman, Z. Szotek, A. Ernst, and H. Winter, Phys. Rev. B **66**, 064434 (2002).

[21] M. M. Otrokov, A. Ernst, S. Ostanin, G. Fischer, P. Buczek, L. M. Sandratskii, W. Hergert, I. Mertig, V. M. Kuznetsov, and E. V. Chulkov, Phys. Rev. B **83**, 155203 (2011).

[22] J. Staunton, B. L. Gyorffy, A. J. Pindor, G. M. Stocks, and H. Winter, J. Phys. F: Met. Phys. **15**, 1387 (1985).

[23] S. Shallcross, A. E. Kissavos, V. Meded, and A. V. Ruban, Phys. Rev. B **72**, 104437 (2005).

[24] D. J. Singh, J. Appl. Phys. **79**, 4818 (1996).

[25] I. I. Mazin and D. J. Singh, Phys. Rev. B **56**, 2556 (1997).

[26] J. B. Goodenough, *Magnetism and the Chemical Bond* (Wiley, New York, 1993).

[27] A. G. Petukhov, I. I. Mazin, L. Chioncel, and A. I. Lichtenstein, Phys. Rev. B **67**, 153106 (2003).

[28] D. Böttcher, A. Ernst, and J. Henk, J. Magn. Magn. Mater. **324**, 610 (2012).

[29] T. Wolfram and S. Ellialtioglu, *Electronic and Optical Properties of d-Band Perovskites* (Cambridge University Press, Cambridge, 2006).